




Citrobacter amalonaticus Inhibits the Growth of *Citrobacter rodentium* in the Gut Lumen

Caroline Mullineaux-Sanders,^a Danielle Carson,^a Eve G. D. Hopkins,^a Izabela Glegola-Madejska,^a Alejandra Escobar-Zepeda,^{b,c} Hilary P. Browne,^c Trevor D. Lawley,^c  Gad Frankel^a

^aCentre for Molecular Microbiology and Infection, Department of Life Sciences, Imperial College, London, United Kingdom

^bMicrobiome Informatics Team, EMBL-EBI, Hinxton, United Kingdom

^cHost-Microbiota Interactions Lab, Wellcome Trust Sanger Institute, Hinxton, United Kingdom

ABSTRACT The gut microbiota plays a crucial role in susceptibility to enteric pathogens, including *Citrobacter rodentium*, a model extracellular mouse pathogen that colonizes the colonic mucosa. *C. rodentium* infection outcomes vary between mouse strains, with C57BL/6 and C3H/HeN mice clearing and succumbing to the infection, respectively. Kanamycin (Kan) treatment at the peak of C57BL/6 mouse infection with Kan-resistant *C. rodentium* resulted in relocalization of the pathogen from the colonic mucosa and cecum to solely the cecal luminal contents; cessation of the Kan treatment resulted in rapid clearance of the pathogen. We now show that in C3H/HeN mice, following Kan-induced displacement of *C. rodentium* to the cecum, the pathogen stably colonizes the cecal lumens of 65% of the mice in the absence of continued antibiotic treatment, a phenomenon that we term antibiotic-induced bacterial commensalization (AIBC). AIBC *C. rodentium* was well tolerated by the host, which showed few signs of inflammation; passaged AIBC *C. rodentium* robustly infected naive C3H/HeN mice, suggesting that the AIBC state is transient and did not select for genetically avirulent *C. rodentium* mutants. Following withdrawal of antibiotic treatment, 35% of C3H/HeN mice were able to prevent *C. rodentium* commensalization in the gut lumen. These mice presented a bloom of a commensal species, *Citrobacter amalonaticus*, which inhibited the growth of *C. rodentium* *in vitro* in a contact-dependent manner and the luminal growth of AIBC *C. rodentium* *in vivo*. Overall, our data suggest that commensal species can confer colonization resistance to closely related pathogenic species.

IMPORTANCE Gut bacterial infections involve three-way interactions between virulence factors, the host immune responses, and the microbiome. While the microbiome erects colonization resistance barriers, pathogens employ virulence factors to overcome them. Treating mice infected with kanamycin-resistant *Citrobacter rodentium* with kanamycin caused displacement of the pathogen from the colonic mucosa to the cecal lumen. Following withdrawal of the kanamycin treatment, 65% of the mice were persistently colonized by *C. rodentium*, which seemed to downregulate virulence factor expression. In this model of luminal gut colonization, 35% of mice were refractory to stable *C. rodentium* colonization, suggesting that their microbiotas were able to confer colonization resistance. We identify a commensal bacterium of the *Citrobacter* genus, *C. amalonaticus*, which inhibits *C. rodentium* growth *in vitro* and *in vivo*. These results show that the line separating commensal and pathogenic lifestyles is thin and multifactorial and that commensals may play a major role in combating enteric infection.

KEYWORDS *Citrobacter*, gastrointestinal infection, colonization resistance

The mammalian gut is colonized by up to 10¹⁴ commensal bacteria, which provide benefits to the host, including *de novo* synthesis of vitamins and metabolism of dietary fibers (1). The microbiota also provides colonization resistance against invading

Citation Mullineaux-Sanders C, Carson D, Hopkins EGD, Glegola-Madejska I, Escobar-Zepeda A, Browne HP, Lawley TD, Frankel G. 2021. *Citrobacter amalonaticus* inhibits the growth of *Citrobacter rodentium* in the gut lumen. mBio 12:e02410-21. <https://doi.org/10.1128/mBio.02410-21>.

Invited Editor Mariagrazia Pizza, GSK Vaccines

Editor Rino Rappuoli, GSK Vaccines

Copyright © 2021 Mullineaux-Sanders et al. This is an open-access article distributed under the terms of the [Creative Commons Attribution 4.0 International license](https://creativecommons.org/licenses/by/4.0/).

Address correspondence to Gad Frankel, g.frankel@imperial.ac.uk.

Received 18 August 2021

Accepted 26 August 2021

Published 5 October 2021

pathogens indirectly by training the host immune system and modulating gut physiology, as well as by competing with or directly killing or arresting the growth of pathogens (2, 3). Successful enteric pathogens are able to overcome the colonization resistance barrier and in many cases exploit the microbiota, for example, by using microbiota-derived metabolites as cues to fine-tune virulence gene expression to the correct niche (2). For example, enterohemorrhagic *Escherichia coli* (EHEC) uses microbiota-derived succinate in the colon to regulate virulence (4). The result is a complex web of interactions between the pathogen and the microbiota, which influences the disease course in a way that may ultimately be beneficial or detrimental to the host.

Enteropathogenic *E. coli* (EPEC), EHEC, and *Citrobacter rodentium* are extracellular enteric pathogens which colonize the intestinal mucosa while forming attaching and effacing (A/E) lesions (5). These are characterized by intimate attachment of the bacteria to intestinal epithelial cells (IECs) and effacement of the brush border microvilli (6, 7). The key virulence factors of A/E pathogens, encoded on the locus of enterocyte effacement (LEE) pathogenicity island, are a type 3 secretion system (T3SS), chaperones, the adhesion intimin, and effector proteins, including Tir (8). Intimin-Tir interactions mediate the intimate bacterial attachment and A/E lesion formation (9, 10). Expression of the LEE genes is regulated by the master regulator Ler (11), which itself is regulated by the LEE-encoded positive and negative regulators GrlA and GrlR, respectively (12), and multiple environmental cues (4, 13). Deletion of *grlR* leads to constitutive expression of Ler and the LEE genes (14).

C. rodentium is a natural murine pathogen which colonizes the colonic mucosa in the presence of the endogenous microbiota. Infection results in the activation of inflammatory and tissue damage repair responses, manifested as diarrhea and colonic crypt hyperplasia (CCH) (5). Susceptibility to *C. rodentium* infection varies between mouse strains. C57BL/6 mice develop a self-limiting infection and mild disease; *C. rodentium* colonization peaks at 6 to 8 days postinfection (DPI), during which time *C. rodentium* adheres to the distal colonic and cecal IECs. The pathogen is subsequently cleared from the mucosa in an IgG-dependent manner at 12 to 14 DPI and then from the lumen via outcompetition by commensals by 21 DPI (15–17). Conversely, C3H-derivative mice are lethally susceptible and typically succumb to diarrheal disease from around 12 DPI (18); mortality in C3H/HeJ mice can be reversed by rehydration therapy (19). Genetic and microbiota variation contributes to differences in disease susceptibility between mouse strains (20), and transplantation of the gut microbiota from Swiss NIH or C57BL/6 mice to C3H/HeJ mice can delay or reverse the mortality phenotype, respectively (21, 22).

We previously demonstrated that treatment with kanamycin (Kan) at the peak of C57BL/6 mouse infection with the bioluminescent and Kan-resistant *C. rodentium* strain ICC180 resulted in a relocalization of the pathogen from the colonic mucosa and cecum to solely the cecal luminal contents, suggesting that Kan-sensitive commensals may be required to sustain *C. rodentium* infection at the colonic mucosa. *C. rodentium* persisted under conditions of continued antibiotic treatment, a phenomenon that we termed antibiotic-induced bacterial persistence (AIBP) (14). Withdrawal of the Kan treatment resulted in rapid clearance of the pathogen (14), presumably as a result of the recovery of the colonization resistance capability of the gut microbiota. Here, we investigated the effect of Kan treatment during *C. rodentium* infection of C3H/HeN (C3H) mice. As with C57BL/6 mice, we found that Kan treatment at the peak of infection causes displacement of the pathogen from the colonic mucosa and cecum to the cecal lumen. However, unlike in C57BL/6 mice, following the withdrawal of Kan treatment, *C. rodentium* was not cleared from 65% of C3H mice but rather continued to persistently colonize the cecal lumen, a phenomenon that we term antibiotic-induced bacterial commensalization (AIBC). Although commensalization did not select for genetically avirulent *C. rodentium* mutants, AIBC *C. rodentium* did not induce acute inflammation in the host. Intriguingly, following the withdrawal of antibiotic treatment, 35% of C3H mice excluded *C. rodentium* from the gut lumen, and we identified a commensal bacterium, *Citrobacter amalonaticus*, which specifically bloomed in these mice.

C. amalonaticus inhibited the growth of *C. rodentium* in a contact-dependent manner *in vitro* and was sufficient to confer colonization resistance against the growth of *C. rodentium* in the gut lumen *in vivo*.

RESULTS

Kan treatment of infected C3H mice induces *C. rodentium* commensalization.

We investigated the effect of Kan treatment during infection of C3H mice with the Kan-resistant and bioluminescent *C. rodentium* strain ICC180. Mice infected with ICC180 were given 7 daily oral Kan treatments from 6 DPI (Fig. 1A). Consistently with previous findings for C57BL/6 mice (14), a single Kan treatment of C3H mice at 6 DPI was sufficient to displace the majority of *C. rodentium* from the colon and cecum to solely the cecum (Fig. 1B), from where *C. rodentium* was shed at approximately 10^8 CFU/g of feces (GoF) for the duration of the treatment period (Fig. 1C). Seventy percent of mice survived until the end of the daily antibiotic treatment (see Fig. S1A in the supplemental material).

Unlike in C57BL/6 mice (14), withdrawal of Kan treatment did not result in complete pathogen clearance. Instead, 65% of surviving mice continued to persistently shed *C. rodentium* at around 10^4 to 10^6 CFU/GoF up to 9 weeks postinfection, when the experiment was terminated (Fig. 1C), a phenomenon that we term antibiotic-induced bacterial commensalization (AIBC). In contrast, 35% of the surviving mice were nonpermissive to AIBC *C. rodentium* and cleared the pathogen (Fig. 1C) (see Materials and Methods for a detailed explanation of the AIBC and nonpermissive criteria). *Ex vivo* bioluminescent imaging (BLI) 9 weeks postinfection demonstrated that AIBC *C. rodentium* resided solely in the cecal and colonic luminal contents (Fig. 1D). Further, while *C. rodentium* was readily identifiable by immunofluorescence staining on the distal colonic mucosas of acutely infected C3H mice, no *C. rodentium* was seen on the distal ileal, proximal colonic, or distal colonic mucosas of mice harboring AIBC *C. rodentium* (Fig. 1E; Fig. S1B). These results demonstrate that following a short Kan treatment course, *C. rodentium* persistently colonizes solely the gut lumen of the majority of C3H mice in the absence of continued antibiotic treatment. However, a minority of the mice were nonpermissive to this long-term colonization, suggesting that the microbiotas in these mice were able to confer resistance to the luminal growth of *C. rodentium*.

The AIBC *C. rodentium* state is not inflammatory. Following the withdrawal of Kan treatment, mice with AIBC *C. rodentium* did not show any visible signs of morbidity and gained weight at a rate similar to that of nonpermissive and uninfected mice (Fig. S2A), suggesting that AIBC *C. rodentium* are nonpathogenic. We therefore investigated whether mice harboring AIBC *C. rodentium* (harvested at 63 DPI; AIBC) displayed characteristic markers of colitis associated with acute *C. rodentium* infection. Nonpermissive mice, acutely infected mice (6 DPI, no treatment; Acute group), mock-infected mice which were mock treated with water from 6 to 12 DPI and harvested at 63 DPI (uninfected plus untreated [UI+UT]), and mock-infected mice which were treated with Kan from 6 to 12 DPI and harvested at 63 DPI (UI+Kan) were used as controls (Fig. 2A).

While the Acute group presented significantly elongated crypts compared to those of UI+UT mice, the UI+Kan group, nonpermissive group, and all but one mouse of the AIBC group showed no hyperplasia (Fig. 2B; Fig. S2B). Overall, the UI+UT and UI+Kan mice showed no change in the levels of LCN-2 (an inflammatory marker) in stools throughout the 63-day experimental period (Fig. S2C). Conversely, AIBC and nonpermissive mice showed an ~30-fold increase in LCN-2 in the stool at 6 DPI, prior to treatment, which decreased steeply at the end of the Kan treatment period (Fig. S2C). Following the withdrawal of Kan treatment in AIBC and nonpermissive mice, LCN-2 levels fluctuated but showed no significant difference from levels in UI+UT mice at 63 DPI (Fig. S2C; Fig. 2C).

Acute *C. rodentium* infection induces global changes in the transcriptome and proteome of IECs (23–25); these changes include an increased expression of the antimicrobial peptide gene *RegIIIγ*, the inducible NO synthase gene *Nos2*, the gamma interferon

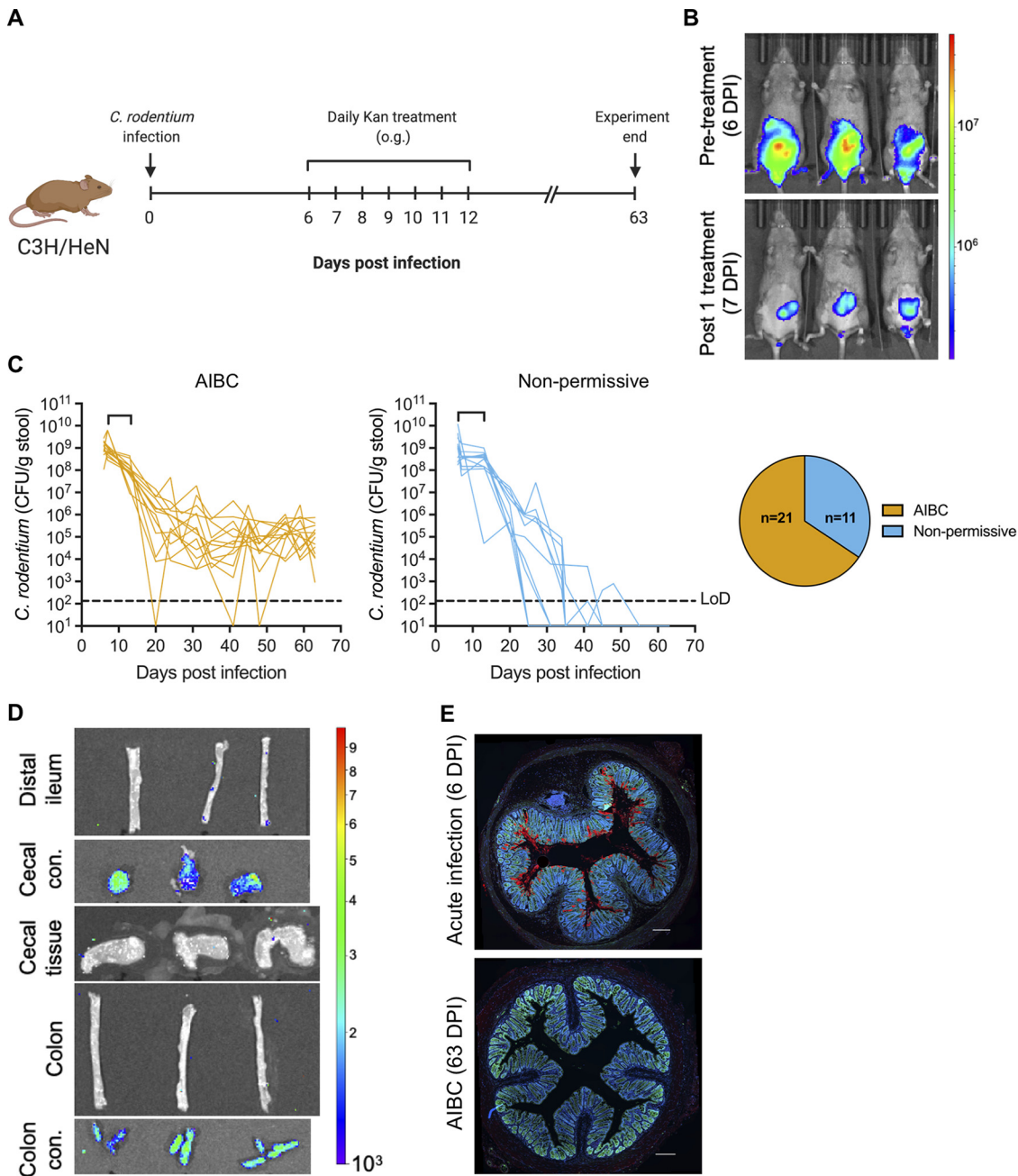


FIG 1 Kan treatment of ICC180-infected C3H mice induces AIBC (A) Schematic of the experimental timeline. o.g., oral gavage. (B) Representative *in vivo* BLIs of mice at 6 DPI prior to Kan treatment (top) and at 7 DPI 24 h after the first Kan treatment (bottom). (C) *C. rodentium* (strain ICC180) colonization of mice designated AIBC (left) or nonpermissive (middle). Brackets on the line graphs denote the Kan treatment period. Each line represents an individual mouse. Only AIBC mice monitored until 63 DPI are shown (24 mice from five biological repeats). (Right, pie chart) The ratio of AIBC to nonpermissive designations of all mice used in this study (32 mice from six biological repeats). LoD, limit of detection. (D) *Ex vivo* BLIs of organs from AIBC mice at 63 DPI. Images are representative of 4 mice from one biological repeat. con., contents. In panels B and D, color scale bar indicates radiance (photons per second per square centimeter per surface radiance). (E) Immunofluorescence staining of the distal colons of mice acutely infected with *C. rodentium* (6 DPI with strain ICC169) or mice harboring AIBC *C. rodentium* at 63 DPI (AIBC), demonstrating no staining of *C. rodentium* on the colonic mucosa in the AIBC group. *C. rodentium*, red; DNA, blue; E-cadherin, green. Images are representative of 8 mice from three biological repeats (AIBC) or 5 mice from one biological repeat (acute infection). Scale bar = 200 μ m.

(IFN- γ)-inducible gene *Ido1*, and the neutrophil chemoattractant gene *Cxcl1*. Quantitative real-time PCR (qRT-PCR) analysis of mRNA from IECs from UI+Kan mice showed a mean \log_2 fold change of close to 0 relative to UI+UT mice for all tested genes, suggesting that daily Kan treatment from 6 to 12 DPI did not influence the expression of these

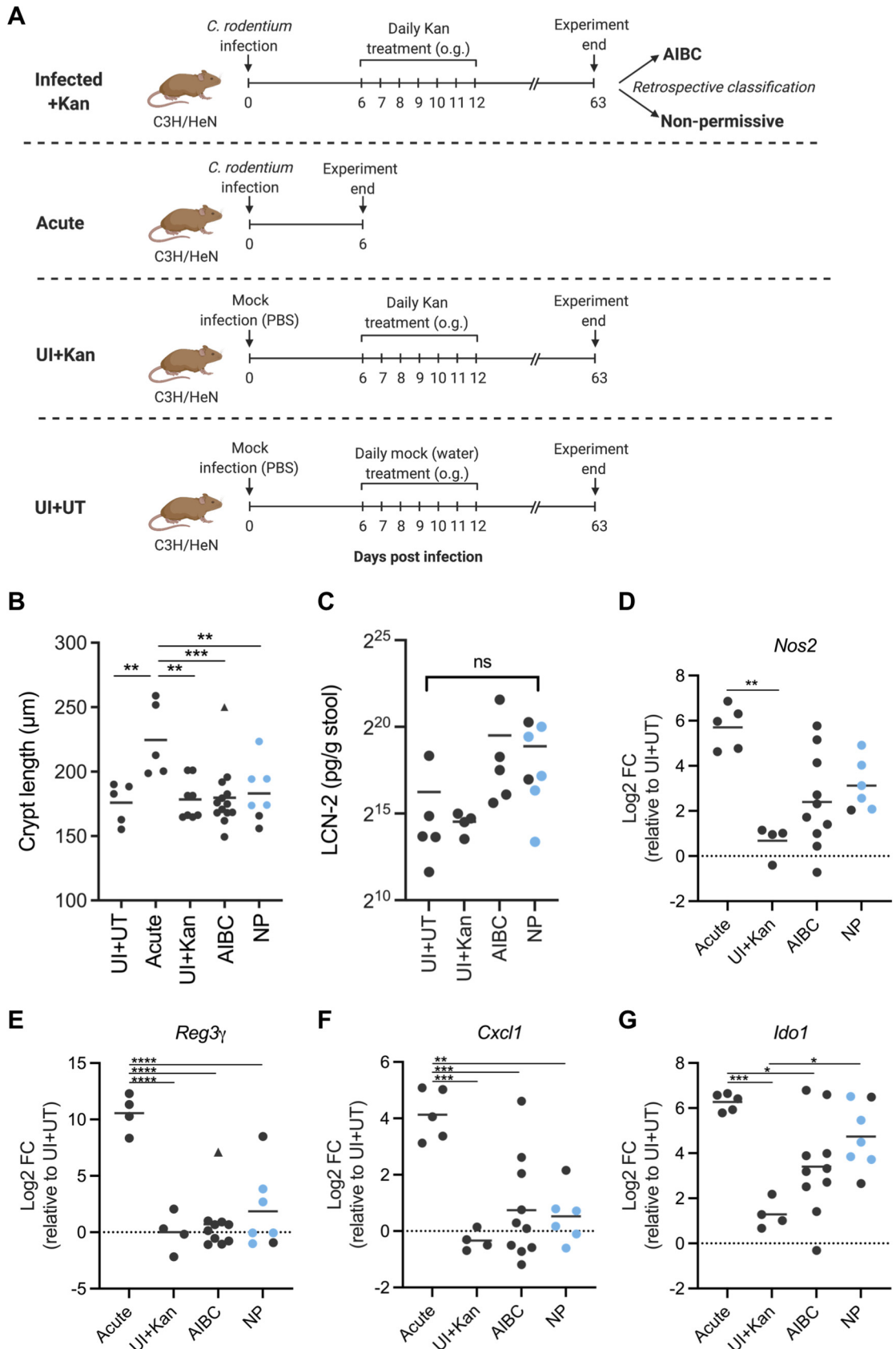


FIG 2 AIBC *C. rodentium* is not inflammatory. (A) Schematic of the experimental timeline of the AIBC, nonpermissive, Acute, UI+Kan, and UI+UT groups of mice. AIBC and nonpermissive mice are the same mice shown in Fig. 1C. (B) Colonic crypt lengths (Continued on next page)

genes at 63 DPI. As expected, Acute group mice had a significantly higher expression of *RegIIIγ*, *Ido1*, *Nos2*, and *Cxcl1* than UI+Kan mice (Fig. 2D to G). Conversely, mice harboring AIBC *C. rodentium* showed significantly lower levels of expression than Acute group mice of all the tested genes, except *Nos2* ($P = 0.0513$) (Fig. 2D to G), although with a spread of expression levels that was broader than that of UI+Kan mice (Fig. 2D to G), which likely reflects the gradual resolution of inflammation following an acute infection. Nonpermissive mice showed a transcription profile similar to that of AIBC mice for all tested genes (Fig. 2D to G). Taken together, these results suggest that AIBC *C. rodentium*, which resides in the lumen of the gut, does not induce acute inflammation.

Expression of the LEE is repressed in the AIBC state. A study demonstrated that administering C3H mice a short course of dietary iron promoted insulin resistance, increased intestinal glucose levels, and drove the selection of genetically avirulent *C. rodentium* mutants *in vivo* (26), which persist for long periods in the gut lumen, like AIBC *C. rodentium*. We therefore investigated whether AIBC *C. rodentium* acquired mutations which conferred a loss of LEE gene expression by isolating AIBC *C. rodentium* colonies at 63 DPI and infecting the mouse colonic cell line CMT-93. We found that 100% of passaged AIBC *C. rodentium* colonies isolated at 9 weeks postinfection ($n = 22$ colonies from 5 mice) robustly formed actin-rich pedestals on CMT-93 cells (Fig. 3A), suggesting that they express the T3SS and effector proteins. Consistently, a singly passaged isolate of AIBC *C. rodentium* was able to infect naive C3H mice, which developed a normal colonic infection at 6 DPI (Fig. 3B and C), demonstrating that the AIBC state is not due to a genetic loss of virulence gene function.

As AIBC *C. rodentium* does not acquire genetic mutations preventing LEE gene expression, we next investigated whether *C. rodentium* constitutively expressing the LEE genes could also commensalize. C3H mice were infected with *C. rodentium* Δ *grlR*, which constitutively expresses the LEE genes (14). As with wild-type (WT) *C. rodentium*, a single Kan treatment at 6 DPI caused a relocalization of *C. rodentium* Δ *grlR* from the colon to the cecum (Fig. 3D). However, significantly fewer Δ *grlR* mutant-infected than WT-infected mice survived, with only 40% surviving to the end of the 7-day treatment period (Fig. S1A).

Deletion of the *grlR* gene and, therefore, constitutive expression of the LEE genes confer a fitness cost when *C. rodentium* is grown on LB agar, resulting in colonies which are smaller than WT colonies (Fig. S3A). Interestingly, we noticed that during the Kan treatment period, mice shed notable numbers of the WT-sized large colonies of *C. rodentium* Δ *grlR* in their stool, comprising >75% of the isolated colonies at 13 and 20 DPI (Fig. 3E and F). We therefore hypothesized that *C. rodentium* Δ *grlR* may have acquired genetic mutations during the treatment period preventing the expression of the LEE genes. To test this, we infected CMT-93 cells with large and small colonies isolated at 11 to 20 DPI. While the small-colony strains robustly formed actin-rich pedestals, the large-colony strains were unable to intimately adhere to, or form pedestals on, CMT-93 cells (Fig. 3G). Further, when used to infect naive C3H mice, a large-colony Δ *grlR* isolate was shed at approximately 10^6 CFU/GoF from 3 to 34 DPI (in the absence of antibiotic treatment) (Fig. 3B; Fig. S3B), similar to the level of AIBC *C. rodentium* shedding, and resided in the cecum (Fig. 3C). Taken together, these results suggest that

FIG 2 Legend (Continued)

of mice from the indicated groups. Each point represents the average crypt length of an individual mouse. Data are from one (UI+UT, UI+Kan, Acute), two (nonpermissive), or four (AIBC) biological repeats. (C) Stool LCN-2 concentrations in mice from the indicated groups at 63 DPI. Each point represents an individual mouse. Data are from one (UI+UT, UI+Kan) or two (AIBC, nonpermissive) biological repeats. ns, not significant ($P < 0.05$ for all comparisons, as determined by a one-way ANOVA with Tukey's posttest for multiple comparisons between all groups). (D to G) qRT-PCR analysis of the indicated mRNA isolated from IECs of mice in the Acute, AIBC, nonpermissive, or UI+Kan group. All are shown relative to the mean of results from the UI+UT group. Each point represents an individual mouse. Data are from one (UI+UT, UI+Kan, and Acute), two (NP), or three (AIBC) biological repeats. (B, E to G) *, $P < 0.05$; **, $P < 0.01$; ***, $P < 0.001$; ****, $P < 0.0001$ (as determined by a one-way ANOVA with Tukey's posttest for multiple comparisons between all groups). The triangle points in panels B and E indicate data points identified as an outlier and not included in statistical analyses. (D) *Nos2* data did not pass a normality test and were analyzed by a Kruskal-Wallis test with Dunn's posttest for multiple comparisons between all groups (**, $P < 0.01$). (B to G) Blue points indicate nonpermissive (NP) mice harboring *C. amalonaticus*^{C3H}.

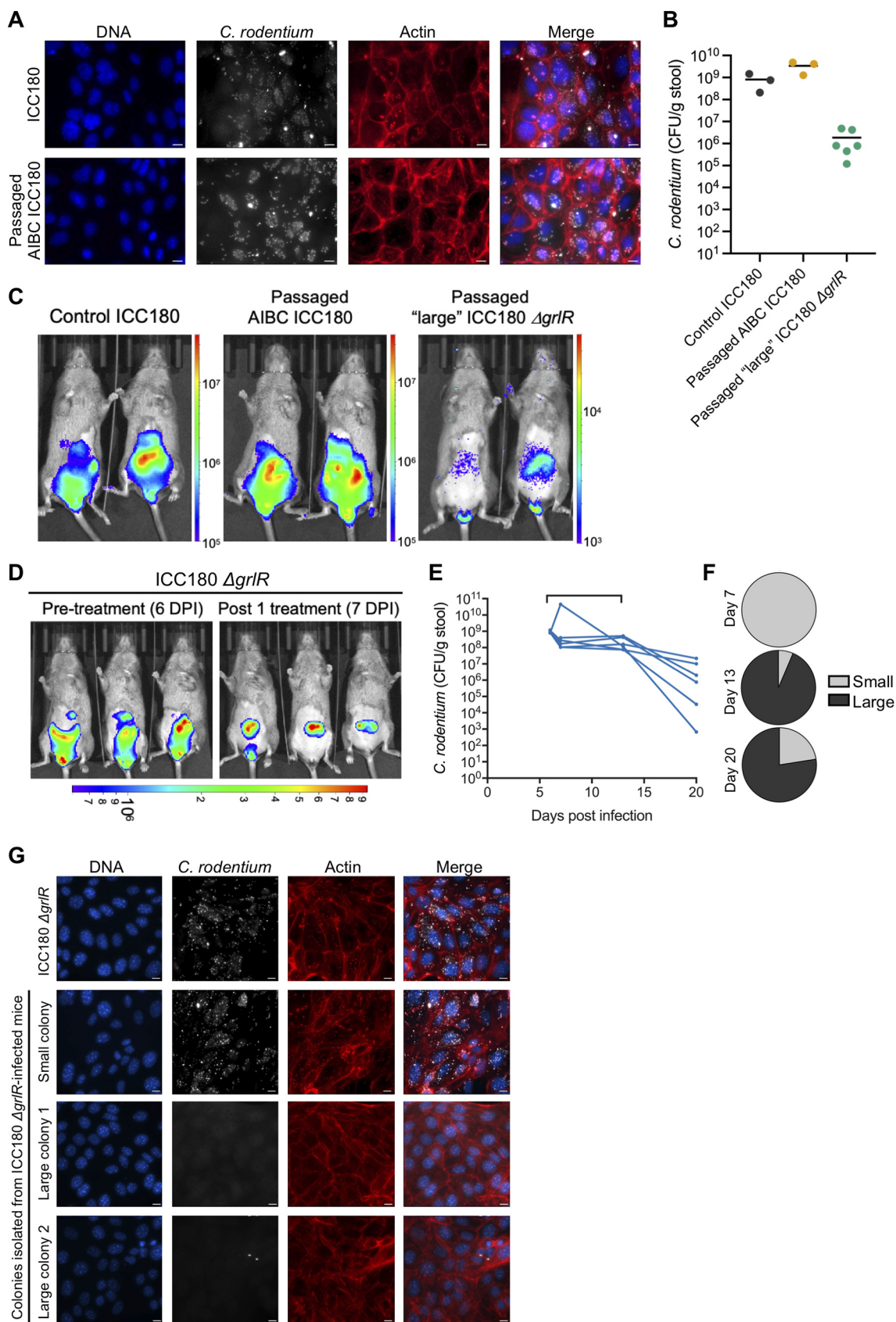


FIG 3 *C. rodentium* T3SS repression is favored in the AIBC state. (A) CMT-93 cells infected with passaged *C. rodentium* isolated from mice with AIBC *C. rodentium* at 63 DPI (mice shown in Fig. 1C). The image is representative of infections with 22 colonies from (Continued on next page)

downregulation of the LEE genes is favored in the AIBC state. Importantly however, in WT *C. rodentium*, the LEE genes are likely downregulated via an active regulatory mechanism, as passaged AIBC *C. rodentium* was able to colonize to WT *C. rodentium* levels, showing no selection for genetic avirulence.

Nonpermissive mice harbor commensal *Citrobacter*. Despite their identical genetic backgrounds, a minority of C3H mice were nonpermissive to AIBC; i.e., *C. rodentium* was cleared once the Kan treatment was stopped (Fig. 1C), suggesting that the microbiotas of these mice provided colonization resistance to the luminal growth of *C. rodentium*. It has been reported that minor facultative anaerobic members of the gut microbiota can vary between genetically similar mouse strains, and this can impact the strains' susceptibility to *Salmonella* infection (27). Further, commensal *E. coli* has been shown to outcompete luminal *C. rodentium* in C57BL/6 mice by competing for monosaccharides (17). We therefore reasoned that a commensal facultative anaerobe may govern permissibility to AIBC. To test this, we cultured fecal facultative commensal anaerobes from the stools of AIBC and nonpermissive mice (following the clearance of *C. rodentium*) on nonselective agar under aerobic conditions. Commensals were similarly cultured from stools of the same mice prior to infection. Colonies were grouped by gross morphology and identified by sequencing of the 16S rRNA gene. Eight out of 10 nonpermissive mice were found to contain a commensal isolate of the *Citrobacter* genus, which was not detectable in any tested AIBC mouse or from any mice (AIBC or nonpermissive) prior to *C. rodentium* infection (Fig. 4A). Nonpermissive mice which harbored commensal *Citrobacter* (blue points in Fig. 2B to G) showed lower levels of inflammatory markers and CCH than mice acutely infected with *C. rodentium*, suggesting that the presence of commensal *Citrobacter* in the gut did not induce acute inflammation.

We generated a high-quality merged Illumina and Nanopore assembly of the genome of a single colony, which demonstrated that it was most closely related to *Citrobacter amalonaticus* based on its full-length 16S rRNA gene, and we named this isolate *C. amalonaticus*^{C3H} (Fig. 4B). *C. amalonaticus*^{C3H} was not isolated from any mouse prior to infection (Fig. 4A), suggesting that, under homeostatic conditions, *C. amalonaticus*^{C3H} is present in the gut below the detection level. The Kan MIC for *C. amalonaticus*^{C3H} was ≤ 8 $\mu\text{g/ml}$ (Fig. S4A), and consistently, the organism bloomed in nonpermissive mice between 13 and 20 DPI (after the withdrawal of Kan treatment) (Fig. S4B), suggesting that a newly created niche following antibiotic depletion of the microbiota may have assisted in its expansion in the gut lumen.

To determine if there were any other changes to the gut microbiota of AIBC and nonpermissive mice, we performed 16S rRNA gene sequencing of fecal samples from AIBC and nonpermissive mice prior to infection (0 DPI) and during the AIBC/nonpermissive states (45 DPI). All groups showed comparable alpha diversities (Fig. S4C). Weighted principal-coordinate analysis (PCoA) showed separate clustering of the 0-DPI and 45-DPI mice, while unweighted PCoA additionally showed separate clustering of the AIBC and nonpermissive groups at 45 DPI (Fig. S4D). Nonpermissive mice showed a higher relative abundance of *Enterobacteriaceae* than AIBC mice, consistent with the observed colonization of nonpermissive mice by *C. amalonaticus* at levels approximately 100-fold higher than those of *C. rodentium* in AIBC mice. Notably, mice had relatively higher levels of S24-7 family

FIG 3 Legend (Continued)

6 mice. Scale bar = 10 μm . (B) *C. rodentium* colonization of mice at 6 DPI with the indicated *C. rodentium* strain. Each point represents an individual mouse. Data are from one (ICC180 and passaged AIBC ICC180) or two (passaged large ICC180 ΔgrlR) biological repeats. (C) Representative *in vivo* BLI images of mice shown in panel B at 6 DPI. (D) *In vivo* BLI images of ICC180 ΔgrlR -infected mice at 6 DPI, prior to Kan treatment (left) and at 7 DPI, 24 h after the first Kan treatment (right). (C, D) Color scale bars indicate radiance (photons per second per square centimeter per surface radiance). (E) *C. rodentium* colonization of mice infected with ICC180 ΔgrlR and treated daily with Kan from 6 to 12 DPI inclusive (denoted by the bracket on the graph). Each line represents an individual mouse, and data are from two biological repeats. (F) Percentages of isolated ICC180 ΔgrlR colonies which were assigned as having a large- or small-colony morphology at the indicated DPI. Pie charts show the average percentages of all mice shown in panel E. (G) CMT-93 cells infected with control ICC180 ΔgrlR or passaged small or large ICC180 ΔgrlR colonies isolated from stool samples of mice shown in panel E at 11 to 20 DPI. Immunofluorescence images are representative of 9 colonies from 5 mice (large colonies) and 8 colonies from 4 mice (small colonies). Scale bar = 10 μm .

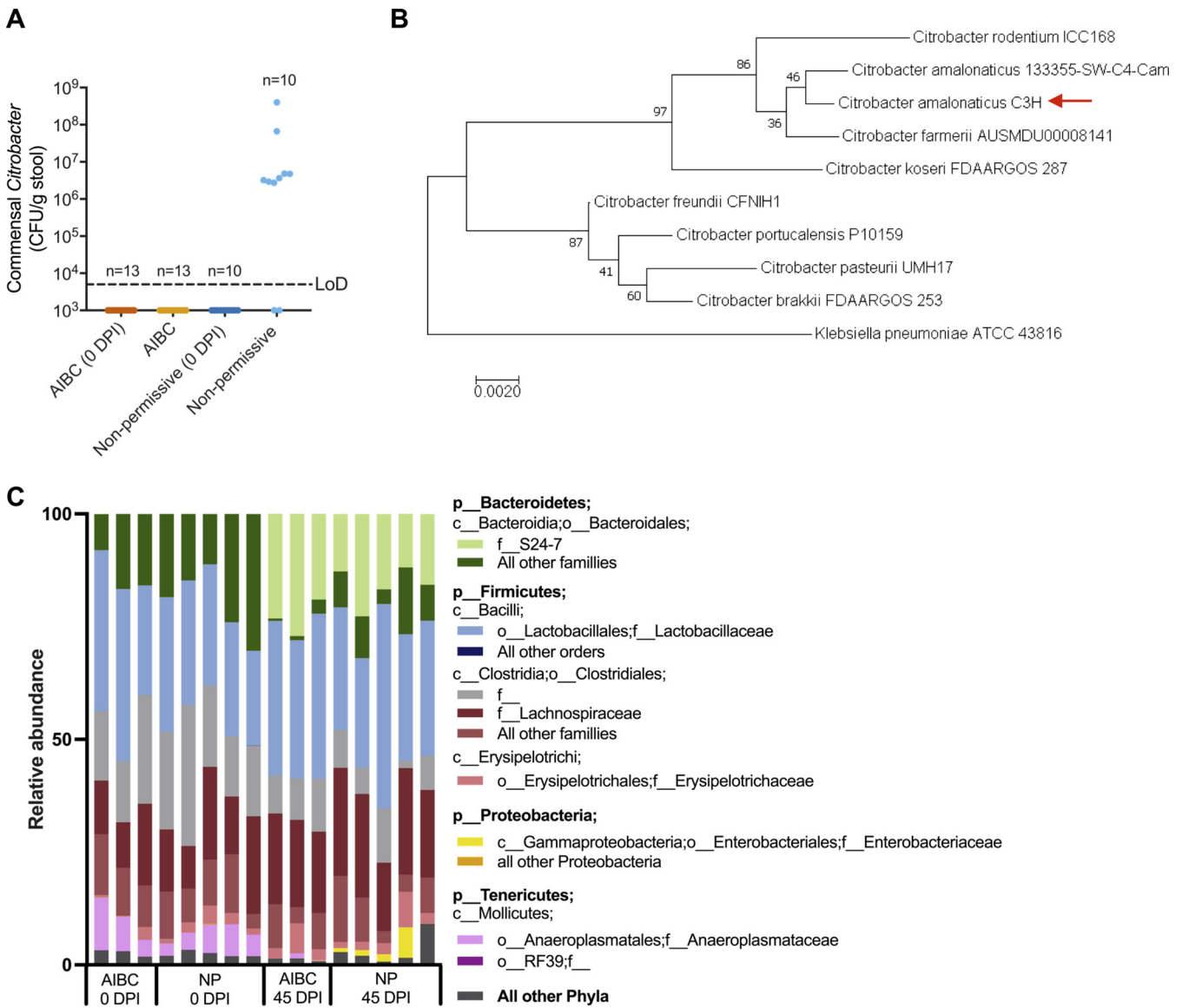


FIG 4 Commensal *Citrobacter* blooms in nonpermissive mice. (A) Non-*C. rodentium* bacteria assigned to the *Citrobacter* genus in stool samples from AIBC and nonpermissive mice collected from the same mice prior to *C. rodentium* infection (0 DPI) and at 34 or 41 DPI. Each point represents an individual mouse. Data are from three biological repeats. LoD, limit of detection. (B) The 16S rRNA gene of *C. amalonaticus*^{C3H} was compared to selected *Citrobacter* species using a maximum likelihood model. The percentage of trees in which the associated taxa cluster together in the bootstrap test (1,000 replicates) is shown next to each branch. The tree is drawn to scale, with branch lengths measured in numbers of substitutions per site. *Klebsiella pneumoniae* is used as an outgroup. The red arrow denotes the *C. amalonaticus*^{C3H} strain isolated in this study. (C) 16S rRNA gene taxonomic analysis of the stool microbiomes from AIBC and nonpermissive (NP) mice at 0 and 45 DPI. Each bar represents a mouse; stool samples from the same mice were analyzed at 0 and 45 DPI. p, phylum; c, class; o, order; f, family.

members and relatively lower levels of *Anaeroplasmataceae* family members at 45 DPI compared to 0 DPI (Fig. 4C). However, these changes were similar between the AIBC and nonpermissive groups, suggesting that this did not impact colonization resistance to *C. rodentium*.

***Citrobacter amalonaticus* governs permissibility to AIBC.** We next tested the ability of *C. amalonaticus*^{C3H} to inhibit *C. rodentium* growth *in vitro*. Coculture on solid agar with *C. amalonaticus*^{C3H} inhibited *C. rodentium* ICC180 growth, as measured by a reduction in bioluminescence (BL) compared to levels after coculture with nonluminescent *C. rodentium* (ICC169) (Fig. 5A), in a temperature-independent manner (Fig. 55A). Further, fluorescence microscopy of cocultures of *C. rodentium* and *C. amalonaticus*^{C3H} expressing either green or red fluorescent protein (GFP or RFP, respectively) also showed inhibition

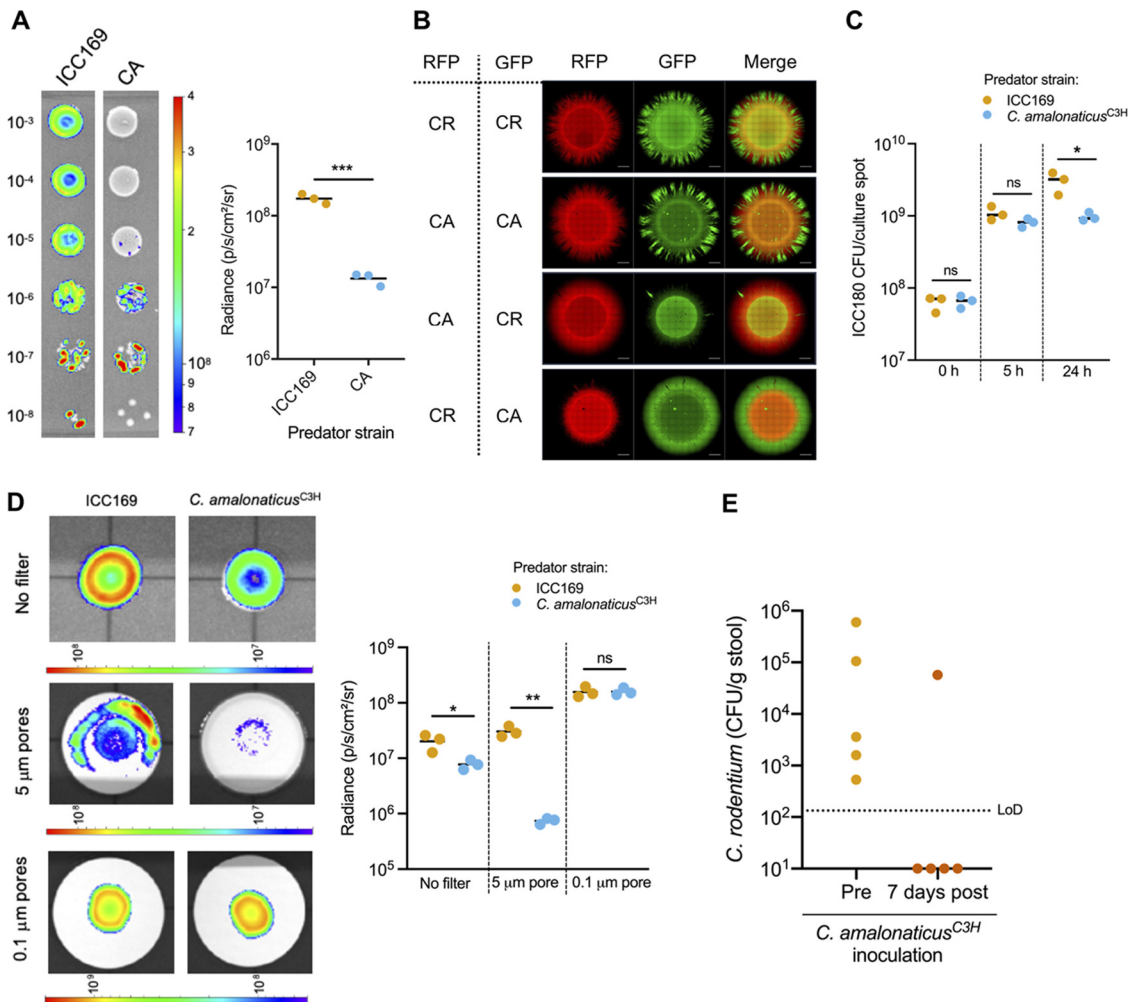


FIG 5 *C. amalonaticus*^{C3H} outcompetes *C. rodentium*. (A, left) Representative BLI of cocultures of ICC180 and ICC169 or *C. amalonaticus*^{C3H} (CA). The number on the left of the cultures indicates the dilution factor. (Right) Graph showing the quantification of BL from the 10⁻³ culture spot of the indicated coculture from three biological repeats. (B) Fluorescence microscopy of cocultures of *C. rodentium* (ICC169; CR) and *C. amalonaticus*^{C3H} (CA) expressing RFP or GFP from a plasmid as indicated after 24 h of growth on LB agar. Scale bar = 1,000 μm. (C) Quantification of ICC180 CFU at 0, 5, and 24 h after coincubation with ICC169 or *C. amalonaticus*^{C3H} (D, left) Representative BLI of ICC180 grown with ICC169 or *C. amalonaticus*^{C3H} separated by a filter with 5-μm or 0.1-μm pores or not separated by a filter. (Right) Graph showing the quantification of BL from the culture spots shown on the left from three biological repeats. (A, C, D) *, *P* < 0.05; **, *P* < 0.01; ***, *P* < 0.001 (as determined by Student's unpaired two-tailed *t* test). (A, D) Color scale bars indicate radiance (photons per second per square centimeter per surface radiance). (E) *C. rodentium* colonization of AIBC mice before (Pre) *C. amalonaticus*^{C3H} inoculation (42 DPI) and 7 days after (post) the first *C. amalonaticus*^{C3H} inoculation (53 DPI). Five mice from one biological repeat were used. LoD, limit of detection.

of *C. rodentium* growth after 24 h (Fig. 5B; Fig. S5B). Quantification of *C. rodentium* ICC180 CFU at 0, 5, and 24 h postinoculation with *C. amalonaticus*^{C3H} on LB agar (LBA) showed ICC180 growth between 0 and 5 h, similar to that observed when ICC180 was grown with ICC169 (nonbioluminescent *C. rodentium*); however, no further growth of ICC180 was observed between 5 and 24 h when cocultured with *C. amalonaticus*^{C3H}, unlike with ICC180 cocultured with ICC169, which continued to grow (Fig. 5C). Together, these results suggest that *C. amalonaticus*^{C3H} inhibits *C. rodentium* growth at high bacterial densities but does not directly kill *C. rodentium*.

Bioluminescent colonies of *C. rodentium* were observed at lower dilutions of the coculture with *C. amalonaticus*^{C3H}, in which single colonies were resolved (Fig. 5A), suggesting that the growth inhibition may be contact dependent. To test this, *C. rodentium* ICC180 was cocultured on agar with either nonluminescent *C. rodentium* or *C. amalonaticus*^{C3H}, with a 0.1-μm-pore-size filter placed between the cultures to allow

the movement of nutrients and secreted products but to restrict direct contact between the bacteria. Filters with 5- μm pores (through which bacteria can traverse) or no filters were placed between the culture spots as controls. *C. rodentium* ICC180 showed significantly lower BL when grown with *C. amalonaticus*^{C3H} than when grown with nonluminescent *C. rodentium* when strains were separated by a 5- μm -pore filter or no filter (Fig. 5D). Conversely, similar bioluminescence was observed from spots of *C. rodentium* ICC180 grown on top of either nonluminescent *C. rodentium* or *C. amalonaticus*^{C3H} when the culture spots were separated by a 0.1- μm -pore filter (Fig. 5D), suggesting that the inhibition of *C. rodentium* growth by *C. amalonaticus*^{C3H} occurs in a contact-dependent manner.

Inspection of the genome sequence of *C. amalonaticus*^{C3H} did not reveal any obvious contact-dependent inhibition machinery (Table S1). While several genes encoding proteins homologous to proteins of the type VI secretion system (T6SS), commonly used in bacterial interspecies competition, were identified, *C. amalonaticus*^{C3H} lacked the full set of core components required to encode a functional T6SS (28). Indeed, *C. amalonaticus*^{C3H} strains with single deletions of genes encoding proteins homologous to the T6SS Hcp (*ctsH4_2*), TssM (00759), or VgrG (03332) components or RHS toxin-like protein (*wapA_4*), encoded adjacent to TssM, did not show a reduced ability to inhibit *C. rodentium* growth (Fig. S5C). Therefore, the molecular mechanism by which contact-dependent growth inhibition occurs requires further investigation.

We next tested whether *C. amalonaticus*^{C3H} could reverse AIBC *C. rodentium* *in vivo*. A single colony, isolated from an uninfected C57BL/6 mouse and identified by 16S rRNA gene sequencing as the *Escherichia-Shigella* genus (referred to as *Escherichia*^{C57}), was used as a control. In an initial experiment, 3 mice (harboring AIBC *C. rodentium* at 42 DPI and negative for *C. amalonaticus*^{C3H}) were orally administered two inoculations of $\sim 1 \times 10^9$ CFU *Escherichia*^{C57} (on DPI 42 and 44). *Escherichia*^{C57} persistently colonized the mice at a level similar to that of AIBC *C. rodentium*; however, this did not alter *C. rodentium* colonization up to 13 days after gavage (55 DPI) (Fig. S5D). These mice were subsequently orally administered two inoculations of *C. amalonaticus*^{C3H} (on DPI 55 and 57). *C. amalonaticus*^{C3H} colonized the mice at around 10^7 CFU/GoF, similar to levels observed in naturally nonpermissive mice. Further, 2 of the 3 mice cleared *C. rodentium* 7 days following administration of *C. amalonaticus*^{C3H} (62 DPI) (Fig. S5D). Next, to ensure that this effect was a result of *C. amalonaticus*^{C3H} alone (rather than the combined effect of *Escherichia*^{C57} and *C. amalonaticus*^{C3H}), 5 mice (harboring AIBC *C. rodentium* at 42 DPI and negative for *C. amalonaticus*^{C3H}) were given two inoculations of *C. amalonaticus*^{C3H} (at 42 and 43 DPI). Again *C. amalonaticus*^{C3H} colonized at around 10^7 CFU/GoF, and 4 of the 5 mice cleared *C. rodentium* 7 days following administration of *C. amalonaticus*^{C3H} (Fig. 5E; Fig. S5E). Overall, these results suggest that under the conditions of our model, the commensal *C. amalonaticus*^{C3H} is sufficient to confer colonization resistance to the growth of luminal *C. rodentium*.

DISCUSSION

Enteric pathogens use both host- and microbiota-derived cues to control virulence gene expression and metabolism, which allows them to compete with and/or evade the microbiota and colonize their host (2, 29). Conversely, the gut microbiota assists the host in clearing invading pathogens through a process known as colonization resistance (17). Here, we identify the commensal bacterium *C. amalonaticus*^{C3H} as capable of inhibiting luminal *C. rodentium* growth *in vivo*. While previous studies have implicated commensal *E. coli* in outcompeting *C. rodentium* via nutrient deprivation (17), our study identifies an intragenus competition in which *C. amalonaticus*^{C3H} employs a contact-dependent mechanism to inhibit *C. rodentium* growth.

We find that a short Kan treatment course that induces taxonomic changes to the gut microbiota (14) and changes the anatomical localization of *C. rodentium* within the host results in the pathogen adopting a commensal lifestyle in C3H mice following cessation of the antibiotic treatment. The persistent growth of WT *C. rodentium* in the gut

for long periods of time has previously been observed in germfree C57BL/6 mice (17) and in specific-pathogen-free (SPF) C57BL/6 mice under conditions of continuous Kan treatment (AIBP) (14). While it has been demonstrated that host diet alteration can select for genetically attenuated *C. rodentium* in C3H mice (26), we did not find evidence of acquisition of genetic mutations preventing T3SS function in WT *C. rodentium* in our luminal-colonization model. Conversely, *C. rodentium* harboring mutations in the LEE sequence were dominant following the 7-day Kan treatment period during infection with *C. rodentium* Δ *grlR*, which expresses these genes constitutively, suggesting that WT *C. rodentium* rapidly downregulates its LEE gene expression in the lumen, while the Δ *grlR* strain, which cannot modulate expression through regulation, achieves this through genetic mutation. While repression of *ler* in WT *C. rodentium* during AIBC remains to be directly shown, it has previously been demonstrated to occur during germfree mouse infection and during AIBP (14, 17). Understanding the signals which govern this virulence gene expression switch may provide a mechanism by which pathogen virulence can be attenuated *in vivo*.

Interestingly, despite persisting in the host following the withdrawal of Kan treatment, AIBC *C. rodentium* remains in the cecal luminal contents and does not recolonize the colonic mucosa, its physiological infection niche. It is possible that the cues required for LEE expression (and therefore mucosal colonization) are absent in the cecum following Kan treatment or that following the initial acute infection, the mucosa is refractory to recolonization by *C. rodentium*. During acute infection, LEE gene expression likely confers an advantage *in vivo* by allowing *C. rodentium* to colonize the mucosa, therefore allowing it to avoid competition with the luminal microbiota; however, expression is costly, and therefore under nonadvantageous conditions (e.g., the gut lumen) and in the absence of competitors, *C. rodentium* coexists with the host asymptotically. It is notable that during Kan treatment (and during colonization of germfree mice [17]), *C. rodentium* colonizes at around 10^8 to 10^9 CFU/GoF, but during AIBC, this falls to around 10^5 CFU/GoF, a colonization level previously reported for facultative anaerobic members of the microbiota (27). This suggests that 10^5 CFU/GoF is the maximum *C. rodentium* colonization level that can be sustained in the context of the polymicrobial community of the cecal lumen.

We found that, following cessation of antibiotic treatment, a minority of C3H mice were refractory to the luminal growth of *C. rodentium*, suggesting that the microbiotas of these mice provided colonization resistance; we identified a commensal facultative anaerobe, *C. amalonaticus*^{C3H}, which governs this. Similarly, differences in commensal species between genetically similar or identical mice have been reported to confer differences in susceptibility to *Salmonella* infection and dextran sulfate sodium (DSS)-induced colitis (27, 30). *C. amalonaticus*^{C3H} was not detected prior to infection and did not bloom until after withdrawal of the Kan treatment. Antibiotic depletion of the microbiota can create a niche favorable to the expansion of facultative anaerobes post-treatment by altering the nutrient and oxygen availability (31), which may have favored the expansion of *C. amalonaticus*^{C3H}. For example, antibiotic treatment leads to increase oxygenation of the gut by killing butyrate-producing commensals (32, 33). Likewise, during acute infection with *C. rodentium*, IECs switch from ATP production in the mitochondria to aerobic glycolysis, which increases mucosal oxygenation and enables the expansion of closely related species (23). Notably, 20% of nonpermissive mice were also negative for *C. amalonaticus*^{C3H}, which may indicate that there may be other commensals in these mice which are also able to provide colonization resistance against the luminal growth of *C. rodentium* in our model.

Commensal *E. coli* (strain dn15.6244.1) has previously been shown to outcompete avirulent luminal *C. rodentium* in germfree mice by competing for monosaccharides (17). Here, a C57BL/6 stool isolate of the *Escherichia-Shigella* genus was unable to outcompete luminal *C. rodentium* in conventional mice, despite robustly colonizing the gut, suggesting that, unlike with *E. coli* dn15.6244.1, the *Escherichia*^{C57} isolate does not overlap *C. rodentium* in its metabolic requirements. We find that *C. amalonaticus*^{C3H}

inhibits *C. rodentium* growth *in vitro* in a contact-dependent manner, although we cannot rule out the possibility that other growth inhibition mechanisms, such as nutrient competition, may play a role *in vivo*. Contact-dependent killing via a T6SS contributes to commensal-pathogen competition during *Vibrio cholerae* (34), *Shigella sonnei* (35), and enterotoxigenic *Bacteroides fragilis* (36) murine gut infection. It is notable that *C. amalonaticus*^{C3H} colonizes at a ratio of approximately 100 to 1 *C. rodentium* in the lumen, which may allow effective contact-dependent inhibition in the gut lumen.

The line between a pathogenic and commensal organism is a thin one; many members of the microbiota are closely related to classically pathogenic organisms, and the virulence of many bacteria is environment dependent and costly if expressed under nonadvantageous conditions. *C. rodentium* is not a member of the murine gut microbiota; nevertheless, changes in the gut environment can prevent pathogenic behavior, favor downregulation of the LEE genes within the host, and drive it toward a commensal-like lifestyle. We show that commensals closely related to pathogenic bacteria can confer colonization resistance, preventing long-term carriage of enteric pathogens. In the future, growth inhibition by closely related commensals may be exploited to increase colonization resistance against bacterial pathogens to prevent acute infection.

MATERIALS AND METHODS

Bacterial strains and growth. Bacterial strains used in this study are shown in Table S2 in the supplemental material (see also references 37 to 40). Bacteria were grown in lysogeny broth (LB; VWR) at 37°C and with 200-rpm shaking, where required. LB agar (LBA; VWR) was used for growth on solid medium. For cell culture infections, bacteria were grown in low-glucose Dulbecco's modified Eagle's medium (DMEM; Sigma) at 37°C and 5% CO₂. Where required and unless otherwise specified, growth medium was supplemented with the following antibiotics at the indicated concentrations: kanamycin (Kan) at 50 µg/ml, nalidixic acid (Nal) at 50 µg/ml, streptomycin (Sm) at 50 µg/ml, rifamycin (Rif) at 50 µg/ml, gentamicin (Gm) at 10 µg/ml, and chloramphenicol (Cm) at 30 µg/ml.

Animal experiments. Animal experiments were performed in accordance with the Animals Scientific Procedures Act of 1986 (41) and UK Home Office guidelines and were approved by the Imperial College Animal Welfare and Ethical Review Body. Pathogen-free 8- to 10-week-old female C3H/HeN mice and pathogen-free C57BL/6 18- to 20-g female mice were purchased from Charles River Laboratories. Mice were housed in groups of 3 to 5 in individually HEPA-filtered cages with bedding, nesting, and free access to food and water. For each experiment, mice were randomly assigned to experimental groups. Investigators were not blind to the allocation. Mice which lost >20% of their starting weight or became moribund during the experimental period were culled and were excluded from all analyses except for the survival analysis. One mouse was culled for a separate welfare issue and was excluded from all analyses. Mice were infected with approximately 10⁹ CFU *C. rodentium* by oral gavage as previously described (15) or mock infected with 200 µl sterile phosphate-buffered saline (PBS). *C. rodentium* inoculum was retrospectively confirmed by serial dilution and quantification of CFU growth on LBA containing Kan. For Fig. 2, all mice were infected with *C. rodentium* strain ICC180, except for the Acute group mice, which were infected with ICC169. In all other experiments, mice were infected with the strains detailed in the text or figure legends. Where indicated, mice were orally gavaged once daily with Kan (20 mg in sterile water) or mock treated with 200 µl sterile water. For commensal inoculations, mice were inoculated with approximately 10⁹ CFU *C. amalonaticus*^{C3H} or *Escherichia*^{C57}-Rif in 200 µl PBS, prepared as described for *C. rodentium*. Inoculum was retrospectively confirmed by serial dilution and quantification of CFU growth on LBA. For quantification of bacterial shedding, stools were resuspended in 10-ml/g sterile PBS and briefly pelleted (<2-s pulse) to remove large debris, and the supernatant was serially diluted and plated on LBA plus Kan or Nal (*C. rodentium*), LBA plus Rif (*E. coli*^{C57}-Rif), or unsupplemented LBA (*C. amalonaticus*^{C3H}). For *C. amalonaticus*^{C3H} quantification, *Citrobacter* colonies were identified by eye based on their colony morphology, and *C. amalonaticus*^{C3H} was subsequently distinguished from *C. rodentium* ICC180 by bioluminescence imaging (BLI) of the agar plates and exclusion of bioluminescent colonies. Ten colonies identified as *C. amalonaticus*^{C3H} were further confirmed by 16S rRNA gene sequencing, which indicated a 100% accurate identification.

Designation of AIBC and nonpermissive mice. AIBC mice were defined as C3H/HeN mice which, following ICC180 infection and Kan treatment from 6 to 12 DPI, harbored fecal *C. rodentium* ICC180 (detectable by plating on LB agar plus 50 µg/ml Kan at 63 DPI, above the detection threshold of 1.3 × 10² CFU/GoF) without more than one *C. rodentium*-negative sample during the experimental period (until 63 DPI or, where relevant, until mice were inoculated prior to 63 DPI with a commensal). Nonpermissive mice were defined as C3H/HeN mice which, following ICC180 infection and Kan treatment from 6 to 12 DPI, became negative for *C. rodentium* during the experimental period and did not have any subsequent *C. rodentium*-positive stool samples. At least 2 consecutive *C. rodentium*-negative stools samples were obtained at least 7 days apart from nonpermissive mice prior to experiment termination (nonpermissive mice were culled at 34 or 63 DPI). The line graph in Fig. 1C shows *C. rodentium* colonization of AIBC mice followed until 63 DPI without commensal inoculation only; however, all mice designated AIBC (including those subsequently inoculated with commensal species) are included in the pie chart.

BLI. Two-dimensional (2D) bioluminescent imaging of mice, tissue, and agar plates was performed using an IVIS Spectrum CT system (Perkin Elmer). For whole-animal imaging, mice were depilated on their abdomens using hair removal cream prior to the imaging and were maintained under gaseous anesthesia with isoflurane (Zoetis). For tissue imaging, gastrointestinal tissues were excised, the colon was cut longitudinally, the stool was removed with tweezers, the cecal contents were gently removed from the cecal tissue, and the cecal tissue washed briefly in PBS. All tissue was imaged with the mucosa exteriorized. BLI images were processed using the LivingImage software (v4.3.1), and radiance was quantified using the region of interest (ROI) tool.

LCN-2 ELISA. Stool samples were homogenized in 10 ml/g PBS with 0.1% Tween 20 using a vortex machine for 15 min. Samples were centrifuged at 16,000 rpm for 10 min, and the supernatant was extracted and stored at -80°C . The LCN-2 concentration was determined using a DuoSet mouse lipocalin-2 enzyme-linked immunosorbent assay (ELISA) (R&D Systems) according to the manufacturer's instructions.

Histological analysis and immunostaining. Formalin-fixed 0.5-cm whole distal colon, proximal colon, or distal ileum samples were processed, paraffin embedded, and sectioned at $5\ \mu\text{m}$. Formalin-fixed, paraffin-embedded (FFPE) sections were then either stained with hematoxylin and eosin (H&E) by standard techniques or processed for immunofluorescence. For immunofluorescence, sections were dewaxed by submersion in Histo-Clear solution (VWR) twice for 10 min, 100% ethanol twice for 10 min, 95% ethanol twice for 3 min, 80% ethanol once for 3 min, and PBS–0.1% Tween 20–0.1% saponin (PBS-TS) twice for 3 min. Subsequently, sections were heated for 30 min in demasking solution (0.3% trisodium citrate, 0.05% Tween 20 in distilled H_2O). Slides were blocked in PBS-TS supplemented with 10% normal donkey serum (NDS; ThermoFisher Scientific) for 20 min in a humid chamber and then incubated with polyclonal rabbit anti-*C. rodentium* O152 (1:50; Statens Serum Institute, Copenhagen, Denmark) and mouse anti-E-Cadherin antibody (1:50; CD324, BD Biosciences) in PBS-TS–NDS for 1 h. Slides were washed twice for 10 min in PBS-TS, followed by incubation with donkey anti-mouse Alexa Flour 488 (Jackson ImmunoResearch; 1:100) and donkey anti-rabbit Alexa Flour 555 (Jackson ImmunoResearch; 1:100) and Hoechst 33342 stain (1:1,000 dilution). Slides were mounted with ProLong Gold antifade mountant (Thermo Fisher Scientific). Images were acquired using a Zeiss AxioVision Z1 microscope equipped with an AxioCam 105 color camera or Hamamatsu ORCA-Flash 4.0 C11440 camera and processed using Zen 2.3 Blue Version (Carl Zeiss MicroImaging GmbH, Germany). CCH measurements were performed on H&E-stained sections and were obtained from at least 10 well-oriented crypts per mouse.

IEC purification. Colonic IECs were isolated from 3.5-cm distal colonic tissue (following removal of the most distal 0.5-cm tissue for histological analysis), as previously described (24). Briefly, colonic tissue was opened longitudinally and briefly washed in $1\times$ Hanks' balanced salt solution (HBSS) without Mg and Ca. The tissue was incubated at 37°C with shaking for 45 min in enterocyte dissociation buffer ($1\times$ HBSS without Mg and Ca, containing 10 mM HEPES, 1 mM EDTA, and $5\ \mu\text{l/ml}$ 2- β -mercaptoethanol). The remaining tissue was removed, and the lifted enterocytes were subsequently collected by centrifugation ($2,000\times g$ for 10 min), followed by three PBS washes at 4°C . Enterocyte pellets were stored at -80°C .

qRT-PCR. RNA was isolated from purified IECs using the RNeasy minikit (Qiagen) according to the manufacturer's instructions. RNA was treated with RQ1 RNase-free DNase (Promega) for 30 min, and subsequently cDNA was synthesized using a Moloney murine leukemia virus reverse transcription kit (Promega). Amplification from cDNA was performed using Power SYBR green PCR master mix (ThermoFisher Scientific). Assay reactions were performed in a $20\text{-}\mu\text{l}$ volume with $2\times$ Power SYBR green PCR master mix with efficiency-optimized primers to a final concentration of $0.05\ \mu\text{M}$ each and 1 to 10 ng total cDNA. All reactions were carried out in technical duplicates. The $\Delta\Delta C_t$ method (where C_t is threshold cycle) of quantification was performed to give the \log_2 fold change from the expression of averaged baseline measurements (42). Expression was normalized to that of the housekeeping gene *Gapdh*. Primers used are listed in Table S3.

C. rodentium infections of CMT-93 cells. The mouse colonic cell line CMT-93 was grown in high-glucose DMEM (Sigma) supplemented with 10% fetal bovine serum (Gibco), 2 mM glutamine (Gibco), and 1% MEM nonessential amino acids (Sigma) at 37°C with 5% CO_2 . For infections, cells were seeded on glass coverslips in 24-well plates at a concentration of 5×10^4 cells/well and grown for 48 h. Saturated LB *C. rodentium* cultures were diluted 1:100 in low-glucose DMEM (Sigma) and grown overnight at 37°C and 5% CO_2 . One hundred microliters of overnight culture was added to each well. Plates were centrifuged for 5 min at $500\times g$ and incubated at 37°C and 5% CO_2 for 3 h. Cells were then washed three times with sterile PBS, fixed with 4% (wt/vol) paraformaldehyde in PBS for 15 min, quenched with 50 mM NH_4Cl , and permeabilized in 0.1% (vol/vol) Triton X-100 in PBS for 5 min. Coverslips were blocked in PBS supplemented with 1% bovine serum albumin (BSA) for 1 h and then incubated with polyclonal rabbit anti-*C. rodentium* O152 (1:100; Statens Serum Institute, Copenhagen, Denmark) in PBS–BSA for 1 h. Coverslips were washed three times in PBS, followed by incubation with Donkey anti-rabbit Alexa Flour 488 (Jackson ImmunoResearch; 1:200), Phalloidin-iFlour 647 (Strattech; 1:100), and Hoechst 33342 dye or 4',6-diamidino-2-phenylindole (DAPI) (1:1,000) for 1 h. Coverslips were washed three times in PBS and once in distilled H_2O and were mounted with ProLong Gold antifade mountant (Thermo Fisher Scientific). Images were acquired using a Zeiss AxioVision Z1 microscope equipped with a Hamamatsu ORCA-Flash 4.0 C11440 camera and processed using Zen 2.3 (Blue Version) (Carl Zeiss MicroImaging GmbH, Germany).

Commensal bacterial isolation and identification. To isolate commensal bacteria, stool samples were resuspended in 10 ml/g sterile PBS, plated on unsupplemented LBA, and grown at 37°C overnight under atmospheric conditions. *C. rodentium* ICC180 colonies were identified by BLI of the plates, and bioluminescent colonies were excluded. Colonies were grouped based on their colony

morphology and subsequently identified by 16S rRNA gene sequencing of a minimum of 12 colonies/group. For 16S rRNA gene sequencing, individual colonies were resuspended in sterile water containing glass beads and heated at 95°C for 5 min, followed by manual cell disruption using a vortex machine for 10 min. Cell debris was pelleted by brief-pulse centrifugation, and 1 to 5 μ l supernatant used as the template for PCR with primers 16S_27F and 16S_1510R using OneTaq 2 \times master mix (NEB), performed according to the manufacturer's instructions. PCR cleanup and DNA sequencing of the amplified product with the 16S_27F primer was performed by Eurofins. 16S rRNA gene sequences generated from the 16S_27F primer were used to identify the colony genus using the SILVA rRNA gene database "search and classify" function (43). A single isolate of the *Citrobacter* genus was subjected to whole-genome sequencing.

C. amalonaticus^{C3H} whole-genome sequencing. *C. amalonaticus^{C3H}* DNA was isolated using a MasterPure Complete DNA and RNA purification kit (Lucigen). The genome was sequenced on the Illumina HiSeq X 10 platform and Nanopore GridION. Long reads were demultiplexed using qcata v1.1.0 (<https://github.com/nanoporetech/qcata>) and filtered by quality at a minimal Phred score of 10 using NanoFilt v2.5.0 (44). A merged assembly was generated using Unicycler pipeline v0.4.7 (45), with the high-quality long reads and the properly paired reads mapped to an initial version of a long-read assembly generated with Canu v1.6 (46) and Pilon v1.23 (5 rounds) (47). This resulted in a high-quality finished genome that was 4,847,284 bp in length and consisted of one circularized contig. Completeness and contamination were 99.97 and 0.04, respectively, according with CheckM v1.1.2 results (48). Following assembly, the genome was annotated using annotation pipelines at the Wellcome Sanger Institute (49), consisting of gene assignment using PROKKA v1.5 (50) and assignment of gene function by comparison to those of the *Citrobacter amalonaticus* genome from RefSeq (50, 51).

Phylogenetic analysis. Sequences of full-length 16S rRNA genes were obtained for selected *Citrobacter* species from the SILVA rRNA gene database (43) or RefSeq (51) for comparison to the full-length 16S rRNA gene of *C. amalonaticus^{C3H}*. A consensus sequence from multiple 16S rRNA copies within a strain was obtained using the EMBL-EMI EMBOSS-Cons tool (52). Phylogenetic analysis was conducted in MEGA v7.0 (53). The evolutionary history was inferred by using the maximum likelihood method based on the Tamura-Nei model (54). Figure 4B shows the tree with the highest log likelihood (−2851.28). Initial tree(s) for the heuristic search were obtained automatically by applying the Neighbor-Join and BioNJ algorithms to a matrix of pairwise distances estimated using the maximum composite likelihood (MCL) approach and then selecting the topology with the superior log likelihood value. The analysis involved 10 nucleotide sequences. All positions containing gaps and missing data were eliminated. There were a total of 1,521 positions in the final data set.

16S rRNA gene sequencing. DNA was extracted from frozen stool samples using a DNeasy PowerSoil kit (Qiagen). The 16S V4 region was amplified with the 515F and 806R primers. Amplicons were subsequently indexed using the Nexera XT set A (Illumina) primers and sequenced on an Illumina MiSeq with 2 \times 300-bp paired-end reads. Samples were demultiplexed based on sample-specific indices using Illumina RTA software (v1.18.54). Sequences were analyzed using the Qiime2 (version 2020.8) analysis pipeline (55). Demultiplexed FASTA-quality files were used as inputs. Reads were denoised, low-quality reads trimmed, paired-end reads assembled into longer reads, and sequences binned into amplicon sequencing variants using the Dada2 plugin for Qiime2 (56). Alpha and beta diversity analyses were performed using the q2-phylogeny and q2-diversity plugins. Taxonomy was assigned using a naive Bayes classifier trained against the Greengenes 13_8 database, trimmed to contain only the V4 region hypervariable region and preclustered at 99% sequence identity. For taxonomic analysis, any sequences not assigned to the phylum level were excluded.

MIC testing. The MIC of Kan for *C. amalonaticus^{C3H}* was determined by an agar dilution MIC, performed in accordance with published guidance (57). A saturated overnight culture of *C. amalonaticus^{C3H}* was diluted in PBS, and 20 μ l (containing 10⁴ to 10⁵ CFU) was plated on Mueller-Hinton agar (Merck, UK) supplemented with Kan and incubated overnight at 37°C.

Generation of spontaneous antibiotic-resistant commensal mutants. *C. amalonaticus^{C3H}* was isolated from the stool of a nonpermissive C3H/HeN mouse at 41 DPI. *Escherichia^{C57}* was isolated from the stool of an uninfected C57BL/6 mouse. A spontaneous Sm-resistant mutant of *C. amalonaticus^{C3H}* (*C. amalonaticus^{C3H}-SmR*) was obtained by sequentially passaging *C. amalonaticus^{C3H}* on LBA supplemented with increasing concentrations of Sm (10 to 100 μ g/ml). *C. amalonaticus^{C3H}* was then passaged once on unsupplemented LBA before growing once more on LBA supplemented with 100 μ g/ml Sm to ensure selection of a stable Sm-resistant mutant. A spontaneous Rif-resistant mutant of *Escherichia^{C57}* (*Escherichia^{C57}-Rif*) was obtained as described above using Rif concentrations of 5 to 100 μ g/ml.

Electroporation of *Citrobacter* strains. Unless otherwise specified, plasmids were introduced into *C. rodentium* and *C. amalonaticus^{C3H}* via electroporation. Briefly, log-phase bacteria were washed twice and resuspended in 15% glycerol. Approximately 50 to 100 ng of plasmid DNA was added to the cells, and a 2.5-kV pulse was applied (300- Ω resistance, 25- μ F capacitance) to electrocompetent bacteria in 0.2-cm cuvettes through a GenePulser II (Bio-Rad). Bacteria were recovered at 37°C from 200-rpm LB for 1 h and then plated on LBA with appropriate antibiotics to select for transformants.

Construction of gene deletions in *C. amalonaticus^{C3H}*. All gene deletions were constructed on the *C. amalonaticus^{C3H}-SmR* background. All primers used in this study are listed in Table S3. All plasmids used in this study are shown in Table S4 (see also references 58 to 60). Homology regions (HRs) consisting of 500 bp upstream and the first three codons of the gene of interest (GOI; "Up HR") and 500 bp downstream, including the last three codons of the GOI ("Down HR") were amplified by PCR using the primer pairs ...UPHR_F/...UPHR_R and ...DNHR_F/...DNHR_R, respectively, with Q5 high-fidelity 2 \times MasterMix (NEB), according to the manufacturer's instructions. pSEVA612S was linearized using primers

pSEVA612S_F and pSEVA612S_R and joined with the Up and Down HRs using the Gibson Assembly Mastermix (NEB) according to the manufacturer's instructions to create mutator plasmids for individual GOIs. Correct insertion of the up and down HRs into the pSEVA612S plasmid was confirmed by Sanger DNA sequencing (Eurofins) with M13 primers. For gene 03332, a construct of the up and down HRs was synthesized (ThermoFisher) with flanking BamHI- and EcoRI-cut sites and subsequently digested with BamHI and EcoRI (NEB) according to the manufacturer's instructions and then ligated into pSEVA612S digested with BamHI and EcoRI with T4 ligase (NEB) according to the manufacturer's instructions. *C. amalonaticus*^{C3H} gene deletions were created by a two-step recombination process with the relevant pSEVA612S mutator plasmid. pSEVA612S mutator plasmids were introduced to *C. amalonaticus*^{C3H} via tri-parental conjugation. Briefly, 20 μ l of a helper strain, *E. coli* 1047 pRK2013, was incubated with 20 μ l of the donor strain, *E. coli* CC118- λ pir pSEVA612S, for 2 h at 37°C on LBA. Forty microliters of the receiver strain (*C. amalonaticus*^{C3H} harboring pACBSR) was added, and the plate was incubated for 4 h at 37°C. Conjugants were selected on LBA+Gm+Cm. Conjugants were grown in LB+Cm, supplemented with 0.4% L-arabinose for 8 h to induce expression of the I-SceI endonuclease from pACBSR, and subsequently streaked on LB+Sm plates. Cm^r Gm^s colonies (i.e., those in which the pSEVA612S plasmid backbone had successfully been removed) were selected and colonies screened for confirmation of the gene deletion using primers ...Check_F/. . .Check_R by PCR with 2 \times OneTaq Mastermix (NEB) according to the manufacturer's instructions. pACBSR was subsequently removed by passaging strains several times in LB, and bacteria sensitive to Cm were selected.

C. rodentium competition assays. For competition assays performed on solid medium, bacterial strains were prepared by growing single-strain cultures overnight in 5 ml LB supplemented with the appropriate antibiotics at 37°C with 200-rpm shaking. One milliliter of overnight culture was pelleted at 14,000 rpm for 1 min, the supernatant was removed, and the pellet was resuspended in 1 ml fresh LB without antibiotics. For all strains used, this results in a starting culture of approximately 5×10^9 CFU/ml. For each assay, the starting culture density was retrospectively confirmed by serial dilution in PBS and plating on LB containing the appropriate antibiotics.

For bioluminescence competition assays, *C. rodentium* ICC180 was mixed 1:1 with the indicated competitor strain and briefly vortexed, and the mixed culture was serially diluted in sterile PBS and 25 μ l of the 10^{-3} to 10^{-8} dilutions plated in triplicate on LBA (no antibiotics). Plates were incubated for 24 h at the indicated temperature and then subjected to BLI. For contact-dependent assays, 40 μ l (undiluted) competitor strain (*C. rodentium* ICC169 or *C. amalonaticus*^{C3H}) was plated onto LBA and allowed to dry. A 25-mm cellulose nitrile filter with 5- μ m or 0.1- μ m pores (Whatman) was placed over the culture spot, and 20 μ l *C. rodentium* ICC180 (2:1 competitor-to-ICC180 ratio) was placed on top in the center of the filter (or directly on top on the culture spot for the no-filter control). The ICC180 spot was allowed to dry, and plates were incubated for 24 h at 37°C under atmospheric conditions.

For fluorescence competition assays, competitor strains were mixed in a 1:1 ratio and briefly vortexed, and 2 μ l of the mixed culture was plated on LBA+Gm (for maintenance of the fluorophore-expressing pULTRA plasmid). Cultures were incubated at 37°C under atmospheric conditions, and fluorescence images were acquired after 24 h using a Zeiss AxioVision Z1 microscope, processed using the Zen 2.3 blue version (Carl Zeiss Microimaging GmbH, Germany), and photographed after 48 h of growth.

For quantification of ICC180 growth in cocultures, ICC180 (undiluted) was mixed 1:1 with the indicated competitor strain and 20 μ l of the mixed culture placed on top of a 25-mm cellulose nitrile filter with 0.1- μ m pores (Whatman) on a LBA plate. At the indicated time, the filter was removed from the agar plate and placed into a 1.5-ml Eppendorf tube with 1 ml LB and vortexed for 30 s to dislodge bacteria from the filter into the media, which was subsequently serially diluted in sterile PBS and plated on LB+Kan to select for ICC180.

Statistical analysis and data presentation. Data were plotted and statistically analyzed in Prism (version 8). Survival curves were analyzed by a log rank (Mantel-Cox) test. Other data which passed a Kolmogorov-Smirnov or a Shapiro-Wilk normality test were analyzed using a Student unpaired two-tailed *t* test or a one-way ANOVA with Tukey's posttest for comparisons between all groups, as specified. *P* values of <0.05 were considered significant. Where indicated, outliers were identified by the ROUT method. Data that did not pass the specified normality test following identification and removal of outliers were analyzed by a Kruskal-Wallis test with Dunn's posttest for multiple comparisons between all groups. Schematic figures were created using BioRender (BioRender.com).

Data exclusions. Mice which were culled before the experimental endpoint for welfare reasons were excluded from all analysis except for survival analysis (as detailed in "Animal experiments" above). Two mice used as part of this study to test the effect of *C. amalonaticus*^{C3H} inoculation in mice harboring AIBC *C. rodentium* (Fig. S5D) were retrospectively found to have a *C. rodentium*-negative stool sample on the day of intervention with commensal inoculation and were subsequently excluded from all analysis, with the exception of the survival curve analysis. No other mice were excluded from this study.

Data accessibility. The genome assembly of *C. amalonaticus*^{C3H} has been deposited in the NCBI database with the accession number [CP080958](https://doi.org/10.1093/bioinformatics/btq0958).

SUPPLEMENTAL MATERIAL

Supplemental material is available online only.

FIG S1, TIF file, 1.7 MB.

FIG S2, JPG file, 0.9 MB.

FIG S3, TIFF file, 0.9 MB.

FIG S4, TIF file, 0.6 MB.

FIG S5, TIFF file, 1.6 MB.

TABLE S1, XLSX file, 0.3 MB.

TABLE S2, PDF file, 0.1 MB.

TABLE S3, TIF file, 0.9 MB.

TABLE S4, PDF file, 0.1 MB.

ACKNOWLEDGMENTS

We thank Lorraine Lawrence for performing histological tissue processing and staining, Laurence Game and Ivan Andrew at the MRC LMS Genomics Laboratory for 16S rRNA gene next-generation sequencing, and Julia Sanchez-Garrido and Julie A. K. McDonald for critical reading of the manuscript.

This work was supported by grants from the Royal Society and the MRC (G.F. and C.M.-S.). E.G.D.H. is supported by a Wellcome Trust Ph.D. studentship. D.C. was supported by an MRC Ph.D. studentship. T.D.L. and H.P.B. are supported by the Wellcome Trust (grant 098051). A.E.-Z. is funded through an ESPOD fellowship.

We declare no competing interests.

C.M.-S., D.C., E.G.D.H., I.G.-M., A.E.-Z., and H.P.B. performed the experiments and data analysis. G.F. and T.D.L. supervised the project. C.M.-S. and G.F. wrote the paper, with input from all authors.

REFERENCES

- Brestoff JR, Artis D. 2013. Commensal bacteria at the interface of host metabolism and the immune system. *Nat Immunol* 14:676–684. <https://doi.org/10.1038/ni.2640>.
- Bäumler AJ, Sperandio V. 2016. Interactions between the microbiota and pathogenic bacteria in the gut. *Nature* 535:85–93. <https://doi.org/10.1038/nature18849>.
- Thaiss CA, Zmora N, Levy M, Elinav E. 2016. The microbiome and innate immunity. *Nature* 535:65–74. <https://doi.org/10.1038/nature18847>.
- Curtis MM, Hu Z, Klimko C, Narayanan S, Deberardinis R, Sperandio V. 2014. The gut commensal *Bacteroides thetaiotaomicron* exacerbates enteric infection through modification of the metabolic landscape. *Cell Host Microbe* 16:759–769. <https://doi.org/10.1016/j.chom.2014.11.005>.
- Mullineaux-Sanders C, Sanchez-Garrido J, Hopkins EGD, Shenoy AR, Barry R, Frankel G. 2019. *Citrobacter rodentium*-host-microbiota interactions: immunity, bioenergetics and metabolism. *Nat Rev Microbiol* 17:701–715. <https://doi.org/10.1038/s41579-019-0252-z>.
- Knutton S, Lloyd DR, McNeish AS. 1987. Adhesion of enteropathogenic *Escherichia coli* to human intestinal enterocytes and cultured human intestinal mucosa. *Infect Immun* 55:69–77. <https://doi.org/10.1128/iai.55.1.69-77.1987>.
- Mundy R, MacDonald TT, Dougan G, Frankel G, Wiles S. 2005. *Citrobacter rodentium* of mice and man. *Cell Microbiol* 7:1697–1706. <https://doi.org/10.1111/j.1462-5822.2005.00625.x>.
- Shenoy AR, Furniss RCD, Goddard PJ, Clements A. 2018. Modulation of host cell processes by T3SS effectors. *Curr Top Microbiol Immunol* 416:73–115. https://doi.org/10.1007/82_2018_106.
- Crepin VF, Girard F, Schüller S, Phillips AD, Mousnier A, Frankel G. 2010. Dissecting the role of the Tir:Nck and Tir:IRTKS/IRSp53 signalling pathways *in vivo*. *Mol Microbiol* 75:308–323. <https://doi.org/10.1111/j.1365-2958.2009.06938.x>.
- Cepeda-Molero M, Berger CN, Walsham ADS, Ellis SJ, Wemyss-Holden S, Schüller S, Frankel G, Fernández LÁ. 2017. Attaching and effacing (A/E) lesion formation by enteropathogenic *E. coli* on human intestinal mucosa is dependent on non-LEE effectors. *PLoS Pathog* 13:e1006706-23. <https://doi.org/10.1371/journal.ppat.1006706>.
- Mellies JL, Elliott SJ, Sperandio V, Donnenberg MS, Kaper JB. 1999. The Per regulon of enteropathogenic *Escherichia coli*: identification of a regulatory cascade and a novel transcriptional activator, the locus of enterocyte effacement (LEE)-encoded regulator (Ler). *Mol Microbiol* 33:296–306. <https://doi.org/10.1046/j.1365-2958.1999.01473.x>.
- Yang J, Tauschek M, Hart E, Hartland EL, Robins-Browne RM. 2010. Virulence regulation in *Citrobacter rodentium*: the art of timing. *Microb Biotechnol* 3:259–268. <https://doi.org/10.1111/j.1751-7915.2009.00114.x>.
- Pacheco AR, Curtis MM, Ritchie JM, Munera D, Waldor MK, Moreira CG, Sperandio V. 2012. Fucose sensing regulates bacterial intestinal colonization. *Nature* 492:113–117. <https://doi.org/10.1038/nature11623>.
- Mullineaux-Sanders C, Collins JW, Ruano-Gallego D, Levy M, Pevsner-Fischer M, Glegola-Madejska IT, Sägfors AM, Wong JLC, Elinav E, Crepin VF, Frankel G. 2017. *Citrobacter rodentium* relies on commensals for colonization of the colonic mucosa. *Cell Rep* 21:3381–3389. <https://doi.org/10.1016/j.celrep.2017.11.086>.
- Crepin VF, Collins JW, Habibzay M, Frankel G. 2016. *Citrobacter rodentium* mouse model of bacterial infection. *Nat Protoc* 11:1851–1876. <https://doi.org/10.1038/nprot.2016.100>.
- Kamada N, Sakamoto K, Seo SU, Zeng MY, Kim YG, Cascalho M, Vallance BA, Puente JL, Núñez G. 2015. Humoral immunity in the gut selectively targets phenotypically virulent attaching-and-effacing bacteria for intraluminal elimination. *Cell Host Microbe* 17:617–627. <https://doi.org/10.1016/j.chom.2015.04.001>.
- Kamada N, Kim Y-G, Sham HP, Vallance BA, Puente JL, Martens EC, Nunez G. 2012. Regulated virulence controls the ability of a pathogen to compete with the gut microbiota. *Science* 336:1325–1329. <https://doi.org/10.1126/science.1222195>.
- Vallance BA, Deng W, Jacobson K, Finlay BB. 2003. Host susceptibility to the attaching and effacing bacterial pathogen *Citrobacter rodentium*. *Infect Immun* 71:3443–3453. <https://doi.org/10.1128/IAI.71.6.3443-3453.2003>.
- Borenshtein D, Schlieper KA, Rickman BH, Chapman JM, Schweinfest CW, Fox JG, Schauer DB. 2009. Decreased expression of colonic Slc26a3 and carbonic anhydrase IV as a cause of fatal infectious diarrhea in mice. *Infect Immun* 77:3639–3650. <https://doi.org/10.1128/IAI.00225-09>.
- Papapietro O, Teatero S, Thanabalasuriar A, Yuki KE, Diez E, Zhu L, Kang E, Dhillon S, Muise AM, Durocher Y, Marcinkiewicz MM, Malo D, Gruenheid S. 2013. R-Spondin 2 signalling mediates susceptibility to fatal infectious diarrhoea. *Nat Commun* 4:1898. <https://doi.org/10.1038/ncomms2816>.
- Ghosh S, Dai C, Brown K, Rajendiran E, Makarenko S, Baker J, Ma C, Halder S, Montero M, Ionescu VA, Klegeris A, Vallance BA, Gibson DL. 2011. Colonic microbiota alters host susceptibility to infectious colitis by modulating inflammation, redox status, and ion transporter gene expression. *Am J Physiol Gastrointest Liver Physiol* 301:G39–G49. <https://doi.org/10.1152/ajpgi.00509.2010>.
- Willing BP, Vacharaks A, Croxen M, Thanachayanont T, Finlay BB. 2011. Altering host resistance to infections through microbial transplantation. *PLoS One* 6:e26988-10. <https://doi.org/10.1371/journal.pone.0026988>.
- Berger CN, Crepin VF, Roumeliotis TI, Wright JC, Carson D, Pevsner-Fischer M, Furniss RCD, Dougan G, Dori-Bachash M, Yu L, Clements A,

- Collins JW, Elinav E, Larrouy-Maumus GJ, Choudhary JS, Frankel G. 2017. *Citrobacter rodentium* subverts ATP flux and cholesterol homeostasis in intestinal epithelial cells *in vivo*. *Cell Metab* 26:738–752.e6. <https://doi.org/10.1016/j.cmet.2017.09.003>.
24. Hopkins EGDD, Roumeliotis TI, Mullineaux-Sanders C, Choudhary JS, Frankel G. 2019. Intestinal epithelial cells and the microbiome undergo swift reprogramming at the inception of colonic *Citrobacter rodentium* infection. *mBio* 10:e00062–19. <https://doi.org/10.1128/mBio.00062-19>.
25. Carson D, Barry R, Hopkins EGD, Roumeliotis TI, García-Weber D, Mullineaux-Sanders C, Elinav E, Arriemerlou C, Choudhary JS, Frankel G. 2020. *Citrobacter rodentium* induces rapid and unique metabolic and inflammatory responses in mice suffering from severe disease. *Cell Microbiol* 22:e13126–17. <https://doi.org/10.1111/cmi.13126>.
26. Sanchez KK, Chen GY, Schieber AMP, Redford SE, Shokhirev MN, Leblanc M, Lee YM, Ayres JS. 2018. Cooperative metabolic adaptations in the host can favor asymptomatic infection and select for attenuated virulence in an enteric pathogen. *Cell* 175:146–158.e15. <https://doi.org/10.1016/j.cell.2018.07.016>.
27. Velazquez EM, Nguyen H, Heasley KT, Saechao CH, Gil LM, Rogers AWL, Miller BM, Rolston MR, Lopez CA, Litvak Y, Liou MJ, Faber F, Bronner DN, Tiffany CR, Byndloss MX, Byndloss AJ, Bäumlér AJ. 2019. Endogenous Enterobacteriaceae underlie variation in susceptibility to Salmonella infection. *Nat Microbiol* 4:1057–1064. <https://doi.org/10.1038/s41564-019-0407-8>.
28. Navarro-García F, Ruiz-Perez F, Cataldi Á, Larzábal M. 2019. Type VI secretion system in pathogenic *Escherichia coli*: structure, role in virulence, and acquisition. *Front Microbiol* 10:1965–1917. <https://doi.org/10.3389/fmicb.2019.01965>.
29. Connolly JPR, Slater SL, O'Boyle N, Goldstone RJ, Crepin VF, Ruano-Gallego D, Herzyk P, Smith DGE, Douce GR, Frankel G, Roe AJ. 2018. Host-associated niche metabolism controls enteric infection through fine-tuning the regulation of type 3 secretion. *Nat Commun* 9:5148. <https://doi.org/10.1038/s41467-018-07612-0>.
30. Forster SC, Clare S, Beresford-Jones BS, Harcourt K, Notley G, Stares M, Kumar N, Soderholm AT, Adoum A, Wong H, Morón B, Brandt C, Dougan G, Adams DJ, Maloy KJ, Pedicord VA, Lawley TD. 2021. Novel gut pathobionts confound results in a widely used mouse model of human inflammatory disease. *bioRxiv* 2021.02.09.430393.
31. Ng KM, Ferreyra JA, Higginbottom SK, Lynch JB, Kashyap PC, Gopinath S, Naidu N, Choudhury B, Weimer BC, Monack DM, Sonnenburg JL. 2013. Microbiota-liberated host sugars facilitate post-antibiotic expansion of enteric pathogens. *Nature* 502:96–99. <https://doi.org/10.1038/nature12503>.
32. Byndloss MX, Olsan EE, Rivera-Chávez F, Tiffany CR, Cevallos SA, Lokken KL, Torres TP, Byndloss AJ, Faber F, Gao Y, Litvak Y, Lopez CA, Xu G, Napoli E, Giulivi C, Tsolis RM, Revzin A, Lebrilla CB, Bäumlér AJ. 2017. Microbiota-activated PPAR- γ signaling inhibits dysbiotic Enterobacteriaceae expansion. *Science* 357:570–575. <https://doi.org/10.1126/science.aam9949>.
33. Rivera-Chávez F, Zhang LF, Faber F, Lopez CA, Byndloss MX, Olsan EE, Xu G, Velazquez EM, Lebrilla CB, Winter SE, Bäumlér AJ. 2016. Depletion of butyrate-producing *Clostridia* from the gut microbiota drives an aerobic luminal expansion of *Salmonella*. *Cell Host Microbe* 19:443–454. <https://doi.org/10.1016/j.chom.2016.03.004>.
34. Zhao W, Caro F, Robins W, Mekalanos JJ. 2018. Antagonism toward the intestinal microbiota and its effect on *Vibrio cholerae* virulence. *Science* 359:210–213. <https://doi.org/10.1126/science.aap8775>.
35. Anderson MC, Vonaesch P, Saffarian A, Marteyn BS, Sansonetti PJ. 2017. *Shigella sonnei* encodes a functional T6SS used for interbacterial competition and niche occupancy. *Cell Host Microbe* 21:769–776.e3. <https://doi.org/10.1016/j.chom.2017.05.004>.
36. Hecht AL, Casterline BW, Earley ZM, Goo YA, Goodlett DR, Bubeck Wardenburg J. 2016. Strain competition restricts colonization of an enteric pathogen and prevents colitis. *EMBO Rep* 17:1281–1291. <https://doi.org/10.15252/embr.201642282>.
37. Schauer DB, Falkow S. 1993. Attaching and effacing locus of a *Citrobacter freundii* biotype that causes transmissible murine colonic hyperplasia. *Infect Immun* 61:2486–2492. <https://doi.org/10.1128/iai.61.6.2486-2492.1993>.
38. Wiles S, Clare S, Harker J, Huett A, Young D, Dougan G, Frankel G. 2004. Organ specificity, colonization and clearance dynamics *in vivo* following oral challenges with the murine pathogen *Citrobacter rodentium*. *Cell Microbiol* 6:963–972. <https://doi.org/10.1111/j.1462-5822.2004.00414.x>.
39. Herrero M, de Lorenzo V, Timmis K. 1990. Transposon vectors containing non-antibiotic resistance selection markers for cloning and stable chromosomal insertion of foreign genes in Gram-negative bacteria. *J Bacteriol* 172:6557–6567. <https://doi.org/10.1128/jb.172.11.6557-6567.1990>.
40. Figurski DH, Helinski DR. 1979. Replication of an origin-containing derivative of plasmid RK2 dependent on a plasmid function provided in *trans*. *Proc Natl Acad Sci U S A* 76:1648–1652. <https://doi.org/10.1073/pnas.76.4.1648>.
41. UK Government. 1986. Animals Scientific Procedures Act 1986. UK Government, London, United Kingdom. <https://www.legislation.gov.uk/ukpga/1986/14/contents>.
42. Livak KJ, Schmittgen TD. 2001. Analysis of relative gene expression data using real-time quantitative PCR and the 2⁻ $\Delta\Delta$ CT method. *Methods* 25:402–408. <https://doi.org/10.1006/meth.2001.1262>.
43. Quast C, Pruesse E, Yilmaz P, Gerken J, Schweer T, Yarza P, Peplies J, Glöckner FO. 2013. The SILVA ribosomal RNA gene database project: improved data processing and web-based tools. *Nucleic Acids Res* 41:D590–D596.
44. De Coster W, D'Hert S, Schultz DT, Cruts M, Van Broeckhoven C. 2018. NanoPack: visualizing and processing long-read sequencing data. *Bioinformatics* 34:2666–2669. <https://doi.org/10.1093/bioinformatics/bty149>.
45. Wick RR, Judd LM, Gorrie CL, Holt KE. 2017. Unicycler: resolving bacterial genome assemblies from short and long sequencing reads. *PLoS Comput Biol* 13:e1005595. <https://doi.org/10.1371/journal.pcbi.1005595>.
46. Koren S, Walenz BP, Berlin K, Miller JR, Bergman NH, Phillippy AM. 2017. Canu: scalable and accurate long-read assembly via adaptive κ -mer weighting and repeat separation. *Genome Res* 27:722–736. <https://doi.org/10.1101/gr.215087.116>.
47. Walker BJ, Abeel T, Shea T, Priest M, Abouelliel A, Sakthikumar S, Cuomo CA, Zeng Q, Wortman J, Young SK, Earl AM. 2014. Pilon: an integrated tool for comprehensive microbial variant detection and genome assembly improvement. *PLoS One* 9:e112963. <https://doi.org/10.1371/journal.pone.0112963>.
48. Parks DH, Imelfort M, Skennerton CT, Hugenholtz P, Tyson GW. 2015. CheckM: assessing the quality of microbial genomes recovered from isolates, single cells, and metagenomes. *Genome Res* 25:1043–1055. <https://doi.org/10.1101/gr.186072.114>.
49. Page AJ, De Silva N, Hunt M, Quail MA, Parkhill J, Harris SR, Otto TD, Keane JA. 2016. Robust high-throughput prokaryote de novo assembly and improvement pipeline for Illumina data. *Microb Genom* 2:e000083. <https://doi.org/10.1099/mgen.0.000083>.
50. Seemann T. 2014. Prokka: rapid prokaryotic genome annotation. *Bioinformatics* 30:2068–2069. <https://doi.org/10.1093/bioinformatics/btu153>.
51. Pruitt KD, Tatusova T, Brown GR, Maglott DR. 2012. NCBI Reference Sequences (RefSeq): current status, new features and genome annotation policy. *Nucleic Acids Res* 40:D130–D135. <https://doi.org/10.1093/nar/gkr1079>.
52. Madeira F, Park YM, Lee J, Buso N, Gur T, Madhusoodanan N, Basutkar P, Tivey ARN, Potter SC, Finn RD, Lopez R. 2019. The EMBL-EBI search and sequence analysis tools APIs in 2019. *Nucleic Acids Res* 47:W636–W641. <https://doi.org/10.1093/nar/gkz268>.
53. Kumar S, Stecher G, Tamura K. 2016. MEGA7: Molecular Evolutionary Genetics Analysis version 7.0 for bigger datasets. *Mol Biol Evol* 33:1870–1874. <https://doi.org/10.1093/molbev/msw054>.
54. Tamura K, Nei M. 1993. Estimation of the number of nucleotide substitutions in the control region of mitochondrial DNA in humans and chimpanzees. *Mol Biol Evol* 10:512–526. <https://doi.org/10.1093/oxfordjournals.molbev.a040023>.
55. Bolyen E, Rideout JR, Dillon MR, Bokulich NA, Abnet CC, Al-Ghalith GA, Alexander H, Alm EJ, Arumugam M, Asnicar F, Bai Y, Bisanz JE, Bittinger K, Brejnrod A, Brislawn CJ, Brown CT, Callahan BJ, Caraballo-Rodríguez AM, Chase J, Cope EK, Da Silva R, Diener C, Dorrestein PC, Douglas GM, Durall DM, Duvallet C, Edwardson CF, Ernst M, Estaki M, Fouquier J, Gauglitz JM, Gibbons SM, Gibson DL, Gonzalez A, Gorlick K, Guo J, Hillmann B, Holmes S, Holste H, Huttenhower C, Huttley GA, Janssen S, Jarmusch AK, Jiang L, Kaehler BD, Kang K, Keefe CR, Keim P, Kelley ST, Knights D, Koester I, Kosciolk T, et al. 2019. Reproducible, interactive, scalable and extensible microbiome data science using QIIME 2. *Nat Biotechnol* 37:852–857. <https://doi.org/10.1038/s41587-019-0209-9>.
56. Callahan BJ, McMurdie PJ, Rosen MJ, Han AW, Johnson AJA, Holmes SP. 2016. DADA2: high-resolution sample inference from Illumina amplicon data. *Nat Methods* 13:581–583. <https://doi.org/10.1038/nmeth.3869>.
57. Weinstein MP, Patel JB, Burnhman C-A, Zimmer BL. 2018. M07. Methods for dilution antimicrobial susceptibility tests for bacteria that grow aerobically. Approval CDM-A. Clinical and Laboratory Standards Institute, Wayne, PA.

58. Martínez-García E, Goñi-Moreno A, Bartley B, McLaughlin J, Sánchez-Sampedro L, Pascual Del Pozo H, Prieto Hernández C, Marletta AS, De Lucrezia D, Sánchez-Fernández G, Fraile S, De Lorenzo V. 2020. SEVA 3.0: an update of the Standard European Vector Architecture for enabling portability of genetic constructs among diverse bacterial hosts. *Nucleic Acids Res* 48:D1164–D1170. <https://doi.org/10.1093/nar/gkz1024>.
59. Ruano-Gallego D, Álvarez B, Fernández LÁ. 2015. Engineering the controlled assembly of filamentous injectisomes in *E. coli* K-12 for protein translocation into mammalian cells. *ACS Synth Biol* 4:1030–1041. <https://doi.org/10.1021/acssynbio.5b00080>.
60. Mavridou DAI, Gonzalez D, Clements A, Foster KR. 2016. The pUltra plasmid series: a robust and flexible tool for fluorescent labeling of Enterobacteria. *Plasmid* 87–88:65–71. <https://doi.org/10.1016/j.plasmid.2016.09.005>.